Power Optimization of THz Band Heterogeneous Vehicular Networks

Shady.H.A.Samy* , Engy.A.Maher†, Ahmed El-Mahdy‡, Falko Dressler§
The German University in Cairo*†‡, TU Berlin§
Cairo, Egypt
{*shady.armia, †engy.aly, ‡ahmed.elmahdy}@guc.edu.eg
§dressler@ccs-labs.org

***Abstract*—Vehicle-to-everything communication (V2X) is regarded as key component in future vehicular networks and intelligent transportation systems (ITS). V2X features are promising in terms of improving traffic safety, degrading accident rates and offering a new level of comfort for drivers. Mixing the evolution of V2X with the introduction of terahertz (THz) band communication will be envisioned as a salient paradigm to fulfill the rapid development in wireless communication. THz communication promises extensive bandwidth and high-speed communication links among dynamic nodes. In this respect, this paper presents a downlink heterogeneous THz network with Small Cell Base Station (SCBS), Vehicle User Equipments (VUEs), Cellular User Equipment (CUE) and Roadside Unit (RSU). We investigate the optimal power allocation and the signal to interference noise ratio (SINR) for both VUE and CUE. We aim at maximizing the rate for the VUE while satisfying the Quality of Service (QoS) for the CUE. We derive a closed-form expression for the optimal power. Based on the optimal power allocation, we express the overall capacity and study the effect of nodes' location. The numerical results show the effectiveness of THz communication in terms of data rates as well as the performance degradation due to vehicle speed in terms of bit error rate (BER). Moreover, we show how crucial the Direct Link (DL) presence is between the VUEs and compare the optimal power allocation to the equal allocation.**

***Index Terms*—Cooperative communication, DF, HetNet, MRC, Power optimization, Terahertz (THz), V2X.**

I. Introduction

To meet the vast growth in both the amount of data broadband traffic due to the increased number of users and the need for better services quality, network densification will be a key enabler to increase the network capacity. Moving from macrocellular networks to small cells to ultra-dense networks and Heterogeneous Networks (HetNets) [1], supporting 1000-fold higher throughput; boosting the network performance [2].

Over the last few years, wireless data traffic has drastically increased due to the ever increasing demands for high bandwidth connectivity and emerging class of real-time, interactive applications. Nearly twelve percent of global mobile traffic will be on 5G cellular connectivity by 2022 [3] and smartphones will surpass 90% of mobile data traffic by the same year [4]. To meet this tremendous demands of this data deluge, the main objectives for future networks are [5]: 1) support massive amounts of connected devices, 2) extremely high data rates per device (from multiple Gbps up to several Tbps), 3) massive data rates per area, and 4) ultra-reliable transmission to support various critical applications, such as cooperative diversity.

Searching the spectrum below 6 GHz (sub-6 GHz), it is congested and in use by existing mobile networks, broadcasting, satellite communications, and WiFi [6]. Moreover, for mmWave communication systems, such as those at 60 GHz, they can only support data rates in the order of 10 Gbps within one meter which is still two orders of magnitude below the expected requirements[1] [7].

In its turn, THz band communication is envisioned as a key wireless technology to satisfy these objectives, by alleviating the spectrum scarcity and capacity limitations of current wireless systems, and enabling various of long-awaited applications in diverse fields with its high throughput and low latency. The idea of introducing THz band is also a promising candidate to offload traffic from the cellular band and offer better services for short range communicating nodes. Not only does the THz band offer large bandwidth, but it will also allow very high data rates. The THz band is between the microwaves and infrared and it spans the frequencies between 0.1 THz and 10 THz. This band is prominent for vehicular communication since it can support rates up to 1 Tbps in small coverage distance (< 50 m), whereas mmWave has achievable rate greater than 1 Gbps within a range of (< 300 m). Although there are some challenges faced in THz band such as poor propagation characteristics, blockage, absorption loss and spreading loss, researchers have shown that these issues are beneficial in mitigating interference and exhibiting dense deployment of small cells which result in more frequency reuse and increased data security due to higher directionality requirement [8].

According to the US Department of Transportation, vehicle communication can save up to 1,083 lives each year in respect to crashes at intersection and eliminate up to 592,000 accidents involving vehicles [9]. Vehicles will be an integral part of the modern era of communications, having potential to provide ubiquitous connectivity, bring down the number of vehicle crashes, assist in better traffic management, enable variety

This work is supported by the DAAD with funds of the German Federal ministry of education and research, in co-operation between the department of telecommunications systems at TU Berlin and German University in Cairo.

[1]Targeting the data rates offered in THz band which is 1 Tbps.

of applications for road safety and passengers' infotainment, and offer ultra-reliable and low-latency transmissions [10]. Therefore, with the promising side of THz band, many researchers want to shed light on the communication capabilities in vehicles and transportation infrastructures based on vehicle-to-everything (V2X) communications.

A. Related Work

THz communication is expected to play a pivotal role in the upcoming generations of vehicular networks. Therefore, resource management and power optimization have to be studied carefully. The authors in [11] aimed to manage the radio resources while meeting the requirments of VUE and maximizing the sum rate of the CUE. However, they ignored the Doppler effect that has a significant influence on the small-scale fading. Taking into consideration the Doppler effect to represent an accurate model, the authors in [12] focused on maximizing the capacity of VUE while guaranteeing the needs for CUEs, but they used the cellular frequency band. Similarly, the authors in [10] assessed the existing IEEE 802.11p standard and identified the 4G LTE capabilities that are most promising if the perspective of 5G-enabled vehicular communications is adopted. V2X communication technologies evolution and an in-depth technical comparison between 802.11 V2X and cellular V2X was made by authors in [13]. The authors in [14] investigated the impact of weather conditions on mmWave communication and made a study to reveal new insights on mmWave-based V2V communication. The authors in [15] motivated the use of mmWave in V2X communications for its sufficient link quality providing gigabit-per-second data rates with reduced control overhead. In [16], the authors introduced an optimal blind interference alignment scheme for inband vehicular networks, trying to improve the sum rate performance in the finite signal to noise ratio (SNR) regime. With the aim to support both high data rate and extended coverage, the authors in [17] proposed a hybrid IoT network that can dynamically switch between mmWave and THz links to ensure reliable and ultra-fast data connection. Also, a closed-form expression of the interference in THz networks was derived and the coverage probability of THz was evaluated. The authors in [18] proposed an Unmanned Aerial Vehicle (UAV) assisted mobile communication system in THz band with the aim of minimizing the outage probability for optimized power allocation. However, they did not consider the existence of DL communication or even compare the performance with and without the DL and they ignored the mobility. Considering a heterogeneous network environment, the authors in [19] addressed the joint power control and spectrum sharing resources problem for V2X communications based on Long Term Evolution unlicensed (LTE-U) spectrum. Besides, their objective was to maximize the total throughput of CUEs and VUEs while guaranteeing the QoS demands of VUEs. Moreover, the authors in [20] aggregated both the LTE-V and 5G new radio (NR) V2X technology to manage various radio resources to satisfy different user's QoS in heterogeneous vehicle networks.

B. Contributions

To the best of our knowledge, there is no in-depth study for the power optimization in a heterogeneous vehicular network with cellular network in THz band. The main contributions of this paper can be summarized as follows:

- We presented a heterogeneous network with VUEs, RSU and CUEs operating in the THz band and a SCBS which assists the short range communication while being connected to a Macro Cell Base Station (MCBS) in the cellular band. The model used illustrates the V2V and V2I communication groups.
- The QoS for the CUE is guaranteed by considering a certain threshold that should be met even after introducing the VUEs in the same frequency band.
- Depending on the location of the VUE transmitter and the CUE, we studied the power allocation for the system. Also, the overall system capacity is evaluated.
- We obtained the optimum power for the VUE, RSU and SCBS that maximizes the rate of the VUE and offered a closed-form expressions.

II. System and Channel Models

A. System Model

Consider a downlink heterogeneous THz network with a MCBS for wide-area coverage and a SCBS which is placed at the center of a small cell with a certain radius coverage as shown in Fig. 1. The MCBS uses cellular network frequency band in order to offer wider coverage and serve the far away nodes. On the other hand, the SCBS works in the THz frequency band offering higher-speed services with higher capacity than cellular band but with smaller coverage range. Accordingly, the cross-tier interference can be ignored due to the usage of different bands. In addition, the intra-tier interference between SCBSs in other cells can be neglected due the to huge losses in THz channel characteristics.

The model considers two groups, V2V and V2I. V2V group is presented as two vehicle users aiming to share information together, where VUE_i is the vehicle transmitter (Tx) and VUE_k is the vehicle receiver (Rx). Both vehicles are moving with the same speed and in the same direction. For the V2I group, there is a roadside unit (RSU) that carries out its main duty as a decode and forward (DF) relay providing ultra-broadband connectivity.

Moreover, in this single cell, multi-user downlink scenario, the two VUEs are communicating together through the intermediate RSU and directly since the line of sight (LOS) is applicable. The THz frequency band is used for the VUEs, RSU and CUE. Also, the CUE is served by the SCBS. The SCBS is connected to the MCBS through a cellular frequency band.

A receive diversity system is adopted where the VUE_k is able to receive its signal through the direct link (from VUE_i to VUE_k) and from the RSU. Maximal Ratio Combining (MRC) technique is chosen to offer high performance with simultaneous received signals processing.

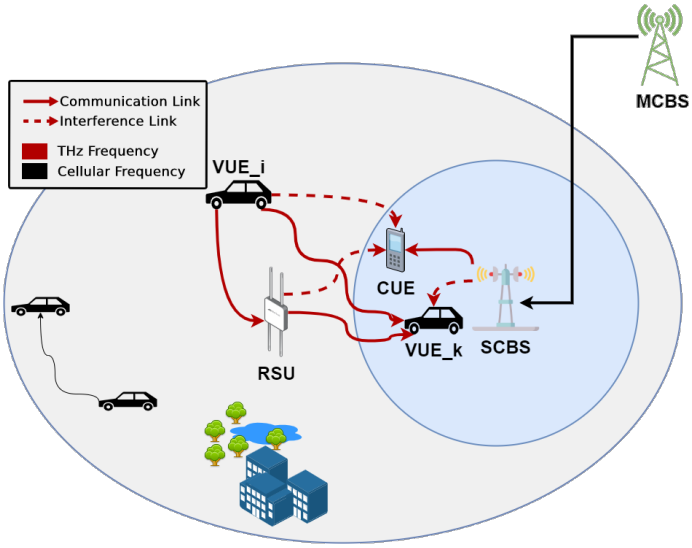

Fig. 1: Downlink HetNet vehicular network in THz band.

This model is close to an urban environment with houses closer to the curb and other significant factors that may block the LOS between the Tx and Rx. The inter-site distance between a Tx and a Rx in this model is preferred not to exceed 50 m since it was found in [21] that at distances equal to 50 m, the maximum transmittance possible is 55% and that can be observed at a certain frequency of 0.8474 THz. For that reason, we considered using this frequency to gain the maximum transmittance possible in case of longer ranges. Also, the bandwidth available at that frequency is around 142 GHz [5].

B. THz Radio Channel Model

The propagation channel can be categorized by a combination of three main effects: path loss, shadowing loss and fading loss. The large scale propagation model is characterized by the first two effects, while the third effect is connected with the small scale propagation model.

Path loss includes the propagation losses which are classified as the sum of two individual losses, namely, the typical spread loss and the absorption loss due to the molecular absorption, that is mainly caused by the water vapour molecules in the atmosphere.

The large-scale fading is given by the effective omnidirectional path loss PL_{eff} which combines the path loss and the shadow fading (SF) [22], [23], [24]. This PL_{eff} is given by:

$$PL_{eff}(d)[dB] = 20\log_{10}\left(\frac{4\pi f_c}{c}\right) + 10\bar{n}\log_{10}(d) + 10\kappa(f)d\log_{10}e + X(0,\sigma) \quad (1)$$

where $\bar{n}$ is the path loss exponent (PLE), c is the speed of light, $\kappa(f)$ is frequency-dependent absorption coefficient and X is the log-normal random SF variable with zero mean and standard deviation σ.

Due to the mobility in the model, the phase (Ψ) consists of the distance-dependent phase change (ϖ) and the velocity-induced Doppler shift (ϑ_D) which influences the small scale fading. This phase is given by:

$$\Psi = \varpi + \vartheta_D \quad (2)$$

$$\Psi = 2\pi\left(f_c \cdot \tau + f_D \cdot \Delta t\right) \quad (2a)$$

$$\Psi = 2\pi\left(f_c\tau + \frac{v_{Rx}\cdot\cos(\phi)}{\lambda}\Delta t\right) \quad (2b)$$

where $\lambda = c/f_c$ is the wavelength, $c = 3\times10^8$ m/s is the speed of light, v_{Rx} is the user speed and f_D is the Doppler frequency which is positive when the user is moving towards the source and negative when moving away from it.

For short inter-site distance of THz communicating nodes, the communication relies heavily on the availability of LOS links due to poor propagation characteristics of the non line of sight (NLOS) links [8]. The probability of having a LOS connectivity is high according to (3) [23].

$$\text{Prob}_{\text{LOS}}(d) = \left[\min\left(\frac{27}{d},1\right)\left(1-e^{-\frac{d}{71}}\right)+e^{-\frac{d}{71}}\right]^2 \approx 1 \quad (3)$$

Hence, the THz channel model can be expressed as:

$$h = \frac{1}{\sqrt{PL_{eff}(d)}}\cdot e^{j2\pi\Psi} \quad (4)$$

where $PL_{eff}(d)$ is given by (1).

III. SINR Evaluation

With a direct LOS connection between the two VUEs, a RSU that carry out DF relaying protocol and a SCBS serving the CUE, the SINR at different nodes will be evaluated in this section. Starting with the SINR at the CUE, it is given as:

$$\hat{\gamma}_{CUE} = \frac{P_{SCBS}\cdot|h_{SCBS,CUE}|^2}{P_{RSU}\cdot|h_{RSU,CUE}|^2 + P_{VUE_i}\cdot|h_{VUE_i,CUE}|^2 + \sigma^2} \quad (5)$$

where $h_{SCBS,CUE}$, $h_{RSU,CUE}$ and $h_{VUE_i,CUE}$ are the THz channels from SCBS to CUE, from RSU to CUE and from VUE_i to CUE, respectively. Moreover, P_{SCBS} is the power of the SCBS, P_{RSU} is the power for the RSU and P_{VUE_i} is the power of VUE_i. The additive noise variance at the CUE is denoted by σ^2.

The SINR for the CUE must be greater than a certain threshold $\Gamma_{\min}$. The threshold is chosen to satisfy the QoS of the CUE so that:

$$\hat{\gamma}_{CUE} \geq \Gamma_{\min} \quad (6)$$

Thus, the power of the SCBS can be written as:

$$P_{SCBS} \geq \frac{\left(P_{RSU}\cdot|h_{RSU,CUE}|^2\cdot\Gamma_{\min}\right)+\left(P_{VUE_i}\cdot|h_{VUE_i,CUE}|^2\cdot\Gamma_{\min}\right)+\left(\Gamma_{\min}\cdot\sigma^2\right)}{|h_{SCBS,CUE}|^2} \tag{7}$$

Since the RSU uses DF relaying protocol, the signal received at RSU and VUE_k for the two links (from VUE_i to RSU and from RSU to VUE_k) can be written respectively as:

$$\hat{\gamma}_1 = \frac{P_{VUE_i}\cdot|h_{VUE_i,RSU}|^2}{\sigma^2} \tag{8}$$

$$\hat{\gamma}_2 = \frac{P_{RSU}\cdot|h_{RSU,VUE_k}|^2}{P_{SCBS}\cdot|h_{SCBS,VUE_k}|^2+\sigma^2} \tag{9}$$

where $h_{VUE_i,RSU}$ is the channel from VUE_i to RSU, h_{RSU,VUE_k} is the channel from the RSU to VUE_k and h_{SCBS,VUE_k} is the channel from SCBS to VUE_k.

The usage of THz band has an influence on the formulation of SINR expressions. This can be noticed in (8) where there is no interference from the SCBS on the RSU due to the poor propagation characteristics and short coverage ranges of THz links.

By comparing the expressions of $\hat{\gamma}_1$ and $\hat{\gamma}_2$, it can be noticed that $\hat{\gamma}_2$ is lower than $\hat{\gamma}_1$ since there is an interference from the SCBS on VUE_k and the channel gain h_{SCBS,VUE_k} is high due to the close separation between SCBS and VUE_k. Besides, the channel gains $h_{VUE_i,RSU}$ and h_{RSU,VUE_k} are almost equal and the power of SCBS is high for the threshold chosen to fulfil the CUE's QoS. Therefore, $\hat{\gamma}_2$ is always lower and the DF relayed link can be now written as:

$$\hat{\gamma}_{VUE_k} = \min\left(\hat{\gamma}_1, \hat{\gamma}_2\right) = \hat{\gamma}_2 \tag{10}$$

Substituting the equality of (7) in (10) gives the expression for $\hat{\gamma}_{VUE_k}$ as:

$$\hat{\gamma}_{VUE_k} = \frac{P_{RSU}\cdot|h_{RSU,VUE_k}|^2\cdot|h_{SCBS,CUE}|^2}{\left\{\left(P_{RSU}\cdot|h_{SCBS,VUE_k}|^2\cdot|h_{RSU,CUE}|^2\cdot\Gamma_{\min}\right)+\left(P_{VUE_i}\cdot|h_{VUE_i,CUE}|^2\cdot|h_{SCBS,VUE_k}|^2\cdot\Gamma_{\min}\right)+\left(|h_{SCBS,VUE_k}|^2\cdot\Gamma_{\min}\cdot\sigma^2\right)+\left(|h_{SCBS,CUE}|^2\cdot\sigma^2\right)\right\}} \tag{11}$$

As shown in Fig. 1, there is no obstruction between VUE_i and VUE_k. Accordingly, the direct LOS component is present and the SINR for this DL can be expressed as:

$$\gamma^{DL}_{VUE_k} = \frac{P_{VUE_i}\cdot|h_{VUE_i,VUE_k}|^2}{P_{SCBS}\cdot|h_{SCBS,VUE_k}|^2+\sigma^2} \tag{12}$$

Substituting the equality of (7) in (12), the direct link can be rewritten as:

$$\gamma^{DL}_{VUE_k} = \frac{P_{VUE_i}\cdot|h_{VUE_i}VUE_k|^2\cdot|h_{SCBS,CUE}|^2}{\left\{\left(P_{RSU}\cdot|h_{SCBS,VUE_k}|^2\cdot|h_{RSU,CUE}|^2\cdot\Gamma_{\min}\right)+\left(P_{VUE_i}\cdot|h_{VUE_i,CUE}|^2\cdot|h_{SCBS,VUE_k}|^2\cdot\Gamma_{\min}\right)+\left(|h_{SCBS,VUE_k}|^2\cdot\Gamma_{\min}\cdot\sigma^2\right)+\left(|h_{SCBS,CUE}|^2\cdot\sigma^2\right)\right\}} \tag{13}$$

The receiving vehicle (VUE_k) uses MRC to combine the received data from the RSU and from VUE_i for joint decoding. Hence, the instantaneous SINR at VUE_k is given by:

$$\underset{MRC}{\hat{\gamma}_{VUE_k}} = \hat{\gamma}_{VUE_k} + \gamma^{DL}_{VUE_k} \tag{14}$$

where $\hat{\gamma}_{VUE_k}$ is the SINR for the relayed link and $\gamma^{DL}_{VUE_k}$ is the SINR for the DL between VUE_i and VUE_k.

For the system model shown in Fig. 1, the overall system data rate can be expressed as:

$$R_{tot} = R_{CUE} + \underset{MRC}{R_{VUE_k}} \tag{15}$$

where R_{CUE} is the data rate for the CUE and $\underset{MRC}{R_{VUE_k}}$ is the rate for VUE_k. From (14), it is noticed that the normalized data rate at VUE_k can be described as:

$$\underset{MRC}{R_{VUE_k}} = R_{VUE_k} + R^{DL}_{VUE_k} \tag{16}$$

where $R_{VUE_k} = \log_2(1+\hat{\gamma}_{VUE_k})$ and $R^{DL}_{VUE_k} = \log_2(1+\gamma^{DL}_{VUE_k})$.

IV. Optimization Problem Derivation

While satisfying the SINR threshold for the CUE, we need to optimize the powers for the RSU, VUE_i and SCBS which are constrained to:

$$P_{SCBS} + P_{RSU} + P_{VUE_i} = P_{MAX} \tag{17}$$

where P_{MAX} is the max power budget for the system.

The optimization problem targets the maximization of the VUE_k data rate in (16), which can be mathematically described after applying the logarithmic property: $\log_a u + \log_a v = \log_a(uv)$ as:

$$\underset{P_{RSU},P_{VUE_i}}{\text{maximize}} \left\{\log_2\left[(1+\hat{\gamma}_{VUE_k})\cdot(1+\gamma^{DL}_{VUE_k})\right]\right\} \tag{18}$$

$$\textbf{s.t:}\ \Big\{P_{RSU}\cdot\left(1+\frac{|h_{RSU,CUE}|^2\cdot\Gamma_{\min}}{|h_{SCBS,CUE}|^2}\right) +P_{VUE_i}\cdot\left(1+\frac{|h_{VUE_i,CUE}|^2\cdot\Gamma_{\min}}{|h_{SCBS,CUE}|^2}\right)\Big\} = P_{MAX}-\frac{\sigma^2\cdot\Gamma_{\min}}{|h_{SCBS,CUE}|^2}\quad , \tag{18a}$$

$$P_{SCBS}>0, P_{RSU}>0, P_{VUE_i}>0\quad , \tag{18b}$$

$$\hat{\gamma}_{CUE}\geq\Gamma_{\min} \tag{18c}$$

It is noted that (18a) is obtained by substituting the equality of (7) in (17). We use Lagrangian method to solve the optimization. Introducing the non-negative Lagrange multiplier λ, we can write the Lagrangian function (F) associated with the problem in (18), after relaxing the power constraint (18a) as:

$$F=\log_2\left[(1+\hat{\gamma}_{VUE_k})\cdot(1+\gamma^{DL}_{VUE_k})\right] -\lambda\big[Z\cdot P_{RSU}+T\cdot P_{VUE_i}-P_t\big] \tag{19}$$

where,

$$Z=1+\frac{|h_{RSU,CUE}|^2\cdot\Gamma_{\min}}{|h_{SCBS,CUE}|^2}$$
$$T=1+\frac{|h_{VUE_i,CUE}|^2\cdot\Gamma_{\min}}{|h_{SCBS,CUE}|^2} \tag{20}$$
$$P_t=P_{MAX}-\frac{\sigma^2\cdot\Gamma_{\min}}{|h_{SCBS,CUE}|^2}$$

To get the optimal power, i.e., P_{RSU} and P_{VUE_i}, we take the partial derivative of F with respect to each power and equate to zero as shown at the top of the next page in (21) and (22).

Solving (21) and (22) for λ, then multiplying both sides by $Q=(B\cdot P_{RSU}+C\cdot P_{VUE_i}+D)$ and simplifying, we get:

$$\begin{aligned}
&\Big\{(P_{RSU}\cdot P_{VUE_i})\cdot\Big[(A\cdot B\cdot C\cdot T)+\big(A\cdot Z\cdot C^2\big)\\
&\quad-\big(E\cdot T\cdot B^2\big)-(E\cdot B\cdot T\cdot A)-(E\cdot B\cdot C\cdot Z)\Big]\Big\}\\
&+\Big\{\big(P^2_{VUE_i}\big)\cdot\Big[\big(A\cdot T\cdot C^2\big)+(A\cdot C\cdot T\cdot E)\\
&\quad-(E\cdot B\cdot C\cdot T)\Big]\Big\}\\
&-\Big\{(P^2_{RSU})\cdot\Big[\big(E\cdot Z\cdot B^2\big)+(A\cdot B\cdot E\cdot Z)\\
&\quad-(A\cdot B\cdot C\cdot Z)\Big]\Big\}\\
&+\Big\{(P_{VUE_i})\cdot\Big[(2\cdot A\cdot D\cdot C\cdot T)+(A\cdot D\cdot T\cdot E)\\
&\quad-(E\cdot D\cdot C\cdot Z)-(E\cdot B\cdot T\cdot D)\Big]\Big\}\\
&+\Big\{(P_{RSU})\cdot\Big[(A\cdot B\cdot D\cdot T)+(A\cdot D\cdot C\cdot Z)\\
&\quad-(A\cdot E\cdot D\cdot Z)-(2\cdot E\cdot B\cdot D\cdot Z)\Big]\Big\}\\
&+\Big[\big(A\cdot T\cdot D^2\big)-\big(E\cdot Z\cdot D^2\big)\Big]=0
\end{aligned} \tag{24}$$

TABLE I: System Parameters

Parameters	Values
Carrier frequency f_c	0.8474 THz
Bandwidth (BW)	2 GHz
Min SINR Threshold for CUE ($\Gamma_{\min}$)	10 dB
Shadow fading $X(\mu,\sigma)$	(0,7) dB
Vehicle User Speed (v_{RX}) (Urban)	30 Km/h
Noise Spectral Density	-174 dBm/Hz
Small BS cell radius	20m
Path-loss exponent $\bar{n}$ [25]	2
P_{MAX}	10 W
Noise variance σ^2	-10 dBm

From (18a) and (20), the power of the transmitting vehicle (P_{VUE_i}) can be described as: $P_{VUE_i}=\frac{P_t}{T}-\frac{Z\cdot P_{RSU}}{T}$, which can be then substituted in (24) and simplified to reach:

$$N\cdot P^2_{RSU}+M\cdot P_{RSU}+W=0 \tag{25}$$

where,

$$\begin{aligned}
N&=\frac{A\cdot C\cdot E\cdot Z^2}{T}\\
M&=\Big[(A\cdot B\cdot C\cdot P_t)-\big(E\cdot B^2\cdot P_t\big)-(E\cdot B\cdot A\cdot P_t)\\
&\quad-\left(\frac{E\cdot B\cdot C\cdot Z\cdot P_t}{T}\right)+\left(\frac{A\cdot C^2\cdot Z\cdot P_t}{T}\right)\\
&\quad+\left(\frac{2\cdot E\cdot B\cdot C\cdot Z\cdot P_t}{T}\right)-\left(\frac{2\cdot A\cdot C^2\cdot Z\cdot P_t}{T}\right)\\
&\quad-\left(\frac{2\cdot A\cdot C\cdot E\cdot Z\cdot P_t}{T}\right)+(E\cdot B\cdot D\cdot Z)\\
&\quad-(2\cdot A\cdot D\cdot C\cdot Z)-(2\cdot A\cdot D\cdot E\cdot Z)\\
&\quad+\left(\frac{E\cdot D\cdot C\cdot Z^2}{T}\right)+(A\cdot B\cdot D\cdot T)\\
&\quad-(2\cdot E\cdot B\cdot D\cdot Z)+(A\cdot D\cdot C\cdot Z)\Big]\\
W&=\left(\frac{A\cdot C^2\cdot P_t^2}{T}\right)-\left(\frac{E\cdot B\cdot C\cdot P_t^2}{T}\right)+\left(\frac{A\cdot C\cdot E\cdot P_t^2}{T}\right)\\
&\quad-(E\cdot B\cdot D\cdot P_t)+(2\cdot A\cdot D\cdot C\cdot P_t)+(A\cdot D\cdot E\cdot P_t)\\
&\quad-\left(\frac{E\cdot D\cdot C\cdot Z\cdot P_t}{T}\right)+\big(A\cdot D^2\cdot T\big)-\big(E\cdot D^2\cdot Z\big)
\end{aligned} \tag{26}$$

The solution for this quadratic equation to get the optimal power for the RSU is expressed as:

$$P^*_{RSU}=\frac{-\Xi\pm\sqrt{\Xi^2-4\cdot\psi\cdot\chi}}{2\psi} \tag{27}$$

Finally, we can get the optimal powers for VUE_i and $SCBS$ from (17) and (18a) while satisfying (18b).

V. Numerical Results and Discussion

In this section, the performance of the system is measured in terms of data rate and BER. The system is simulated and data is transmitted from VUE_i and detected at VUE_k in presence of the interference from SCBS. Then the BER of the detected data is evaluated. The effect of different factors

$$\frac{\partial F}{\partial P_{RSU}} = \left\{ \frac{1}{\left(1+\hat{\gamma}_{VUE_k}\right)\cdot\left(1+\gamma^{DL}_{VUE_k}\right)} \cdot \left[\frac{\left(1+\gamma^{DL}_{VUE_k}\right)\cdot\left(A\cdot C\cdot P_{VUE_i} + A\cdot D\right) - \left(1+\hat{\gamma}_{VUE_k}\right)\cdot\left(E\cdot B\cdot P_{VUE_i}\right)}{\left(B\cdot P_{RSU} + C\cdot P_{VUE_i} + D\right)^2} \right] \right\} - \left(\lambda\cdot Z\right) = 0 \tag{21}$$

$$\frac{\partial F}{\partial P_{VUE_i}} = \left\{ \frac{1}{\left(1+\hat{\gamma}_{VUE_k}\right)\cdot\left(1+\gamma^{DL}_{VUE_k}\right)} \cdot \left[\frac{\left(1+\hat{\gamma}_{VUE_k}\right)\cdot\left(B\cdot P_{RSU} + C\cdot P_{VUE_i} + D\right)\cdot\left(E\right) - \left(C\cdot E\cdot P_{VUE_i}\right) - \left(A\cdot C\cdot P_{RSU}\right) - \left(A\cdot C\cdot \gamma^{DL}_{VUE_k}\cdot P_{RSU}\right)}{\left(B\cdot P_{RSU} + C\cdot P_{VUE_i} + D\right)^2} \right] \right\} - \left(\lambda\cdot T\right) = 0 \tag{22}$$

where,

$$\begin{aligned} A &= \left|h_{SCBS,CUE}\right|^2 \cdot \left|h_{RSU,VUE_k}\right|^2 \\ B &= \left|h_{SCBS,VUE_k}\right|^2 \cdot \left|h_{RSU,CUE}\right|^2 \cdot \Gamma_{\min} \\ C &= \left|h_{VUE_i,CUE}\right|^2 \cdot \left|h_{SCBS,VUE_k}\right|^2 \cdot \Gamma_{\min} \\ D &= \left(\left|h_{SCBS,VUE_k}\right|^2 \cdot \Gamma_{\min}\cdot\sigma^2\right) + \left(\left|h_{SCBS,CUE}\right|^2\cdot\sigma^2\right) \\ E &= \left|h_{VUE_i,VUE_k}\right|^2 \cdot \left|h_{SCBS,CUE}\right|^2 \end{aligned} \tag{23}$$

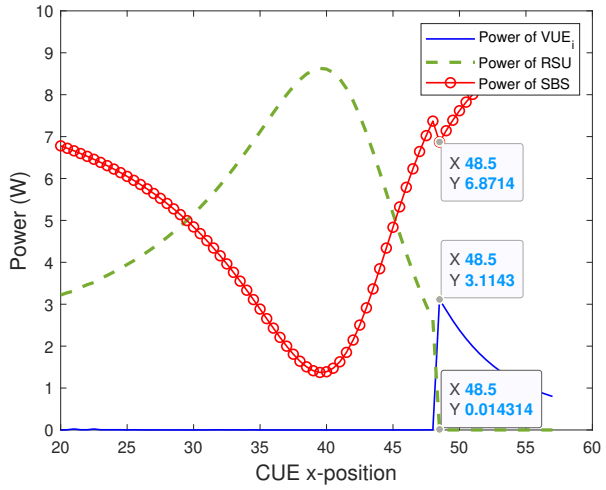

Fig. 2: Power allocation for different CUE location.

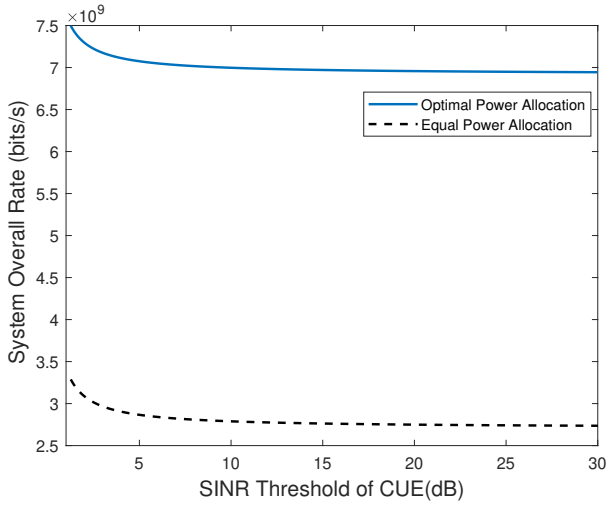

Fig. 3: System overall rate for different CUE Γ_{min}.

such as speed and node location on the system performance and power allocation is studied. The parameters used in the simulations are shown in Table I.

Fig. 2 shows the power versus the location of the CUE relative to other nodes. The coordinate of the SCBS is at (39,19). Therefore, it can be seen that the minimum power for the downlink transmission by the SCBS is at x-position = 39. The reason for this is that the CUE is at the nearest location to the SCBS, thus the minimum power is allocated for the SCBS to satisfy the CUE's QoS. The rest of power is allocated to the RSU and the VUE_i. In this case, more power is allocated to RSU because it is closer to the VUE_k than VUE_i. Moreover, the results show that when the CUE is positioned at 48.5 (9.5m away from the SCBS along x-position), the power is allocated as follows: P_{VUE_i} = 34.93 dBm, P_{RSU} = 11.55 dBm and P_{SCBS} = 38.37 dBm. The P_{RSU} decreases after 48.5m because the CUE starts to get closer to the RSU that interferes on it degrading its QoS. Thus, it is better to allocate more power to VUE_i than RSU.

Fig. 3 represents the system overall rate using the optimal power allocation obtained in section IV versus the SINR threshold of the CUE. Equal power allocation is included for comparison. In equal power allocation, the power budget is distributed equally among the SCBS, RSU, and VUE_i. The figure shows that the optimal power allocation enhanced the system overall rate by around 131 % when compared to the equal power allocation scheme. The overall rate decreases as the threshold increases because it becomes hard for the CUE to satisfy its SINR requirements. Accordingly, the VUE_i and RSU are required to transmit their information with a low

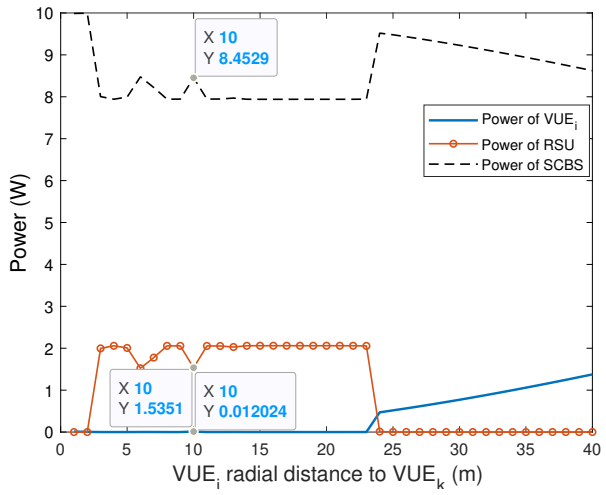

Fig. 4: Power allocation for changeable VUE transmitter location.

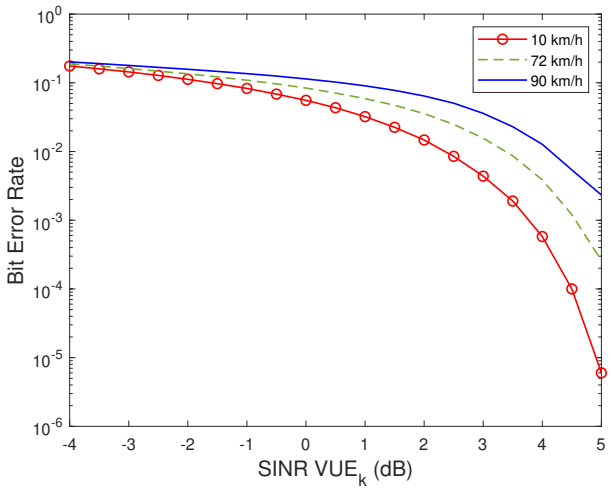

Fig. 5: Speed effect on the bit error rate in case of no direct link between VUE_i and VUE_k.

power. Therefore, the rate of VUE_k decreases; reducing the overall system rate.

Fig. 4 shows the power allocation versus the radial distance from VUE_i to VUE_k. When the distance between the two vehicles is 1m, the power needed for both the VUE_i and RSU is the minimum and most of the power is allocated to the SCBS. Among all points for different power allocations, the threshold Γ_{min} is satisfied for the CUE. When the separation between the two VUEs is 10m, the power is allocated as follows: P_{VUE_i} = 10.80 dBm, P_{RSU} = 31.86 dBm and P_{SCBS} = 39.27 dBm.

Fig. 5 and Fig. 6 are plotted for the case if there is no direct link between the VUE_i and VUE_k due to intermediate obstruction or blockage. Consequently, VUE_k receives its information only through the RSU.

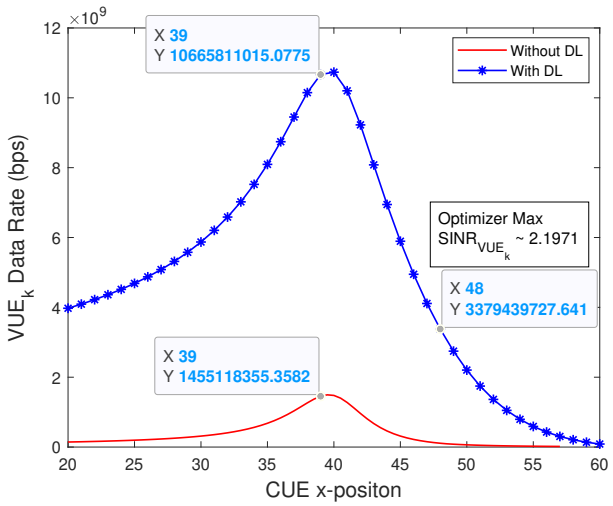

Fig. 6: Data rate at VUE_k with and without DL from VUE_i.

In Fig. 5, we study the effect of changing the speed of the vehicles. The graph illustrates the BER versus the SINR at the VUE_k.The system is simulated by generating a signal with BPSK modulation. The signal is then transmitted over the THz channel. The AWGN and the interference are added to the transmitted signal. On the receiving side, we examined the detected bits to evaluate the error occurred. The results show that the BER decreases as the SINR increases and the increase in vehicle's speed degrades the quality of the received signal due to Doppler effect that affects the channel causing channel fading. For example, at SINR of 2 dB, the BER gets worse by around 77% if the speed increases from 10 km/h to 90 km/h.

Finally, Fig. 6 compares between the data rate at VUE_k with and without direct link between the VUE_i and VUE_k. Both data rates are plotted versus the location of the CUE. As mentioned before, the SCBS is coordinated at (39,19), so when the CUE is located at (39,22), the minimum power is allocated to the SCBS and most of the power budget is given to the RSU and VUE_i that are serving the VUE_k. Therefore, the curve has peak rates at x-coordinate of 39. The rate with DL surpasses the rate without DL by around sixfold increase.

VI. Conclusions

In this paper, we presented a heterogeneous downlink network with VUEs, communicating together through the DL, and RSU in the presence of CUE. The communication is carried in the THz frequency band. We maximized the rate for the VUE while maintaining the requirments for the CUE. Power optimization problem is derived and a closed form expression is expressed. Numerical results were presented to show the importance of power allocation and its effect on the system overall rate. Besides, it showed the relation between BER and vehicle speed, the effect of distance on the power allocation and the significance of the direct link. Finally, THz

communication shall be considered as a new frontier for future vehicular networks.

REFERENCES

[1] C. R. Storck and F. Duarte-Figueiredo, "A survey of 5g technology evolution, standards, and infrastructure associated with vehicle-to-everything communications by internet of vehicles," *IEEE Access*, vol. 8, pp. 117 593–117 614, 2020.

[2] S. H. Samy, E. A. Maher, and A. El-Mahdy, "Full-duplex relay-aided d2d communication in heterogeneous network with imperfect csi," in *2020 16th International Computer Engineering Conference (ICENCO)*, IEEE, 2020, pp. 181–186.

[3] G. Forecast, "Cisco visual networking index: Global mobile data traffic forecast update, 2017–2022," *Update*, vol. 2017, p. 2022, 2019.

[4] S. H. Samy, E. A. Maher, and A. El-Mahdy, "Full-duplex decode and forward relay-aided device-to-device communication," in *2019 Signal Processing: Algorithms, Architectures, Arrangements, and Applications (SPA)*, IEEE, 2019, pp. 131–136.

[5] S. Mumtaz, J. M. Jornet, J. Aulin, W. H. Gerstacker, X. Dong, and B. Ai, "Terahertz communication for vehicular networks," *IEEE Transactions on Vehicular Technology*, vol. 66, no. 7, 2017.

[6] J. Zhang, K. Kang, Y. Huang, M. Shafi, and A. F. Molisch, "Millimeter and thz wave for 5g and beyond," *China Communications*, vol. 16, no. 2, pp. iii–vi, 2019.

[7] I. F. Akyildiz, J. M. Jornet, and C. Han, "Terahertz band: Next frontier for wireless communications," *Physical Communication*, vol. 12, pp. 16–32, 2014.

[8] S. Tripathi, N. V. Sabu, A. K. Gupta, and H. S. Dhillon, "Millimeter-wave and terahertz spectrum for 6g wireless," *arXiv preprint arXiv:2102.10267*, 2021.

[9] M. Noor-A-Rahim, Z. Liu, H. Lee, G. G. M. N. Ali, D. Pesch, and P. Xiao, "A survey on resource allocation in vehicular networks," *IEEE Transactions on Intelligent Transportation Systems*, pp. 1–21, 2020. DOI: 10.1109/TITS.2020.3019322.

[10] S. A. A. Shah, E. Ahmed, M. Imran, and S. Zeadally, "5g for vehicular communications," *IEEE Communications Magazine*, vol. 56, no. 1, pp. 111–117, 2018.

[11] W. Sun, E. G. Ström, F. Brännström, K. C. Sou, and Y. Sui, "Radio resource management for d2d-based v2v communication," *IEEE Transactions on Vehicular Technology*, vol. 65, no. 8, pp. 6636–6650, 2015.

[12] X. Li, L. Ma, Y. Xu, and R. Shankaran, "Resource allocation for d2d-based v2x communication with imperfect csi," *IEEE Internet of Things Journal*, vol. 7, no. 4, pp. 3545–3558, 2020.

[13] H. Zhou, W. Xu, J. Chen, and W. Wang, "Evolutionary v2x technologies toward the internet of vehicles: Challenges and opportunities," *Proceedings of the IEEE*, vol. 108, no. 2, pp. 308–323, 2020.

[14] S. Dimce, M. S. Amjad, and F. Dressler, "Mmwave on the road: Investigating the weather impact on 60 ghz v2x communication channels," in *2021 16th Annual Conference on Wireless On-demand Network Systems and Services Conference (WONS)*, IEEE, 2021, pp. 1–8.

[15] J. Choi, V. Va, N. Gonzalez-Prelcic, R. Daniels, C. R. Bhat, and R. W. Heath, "Millimeter-wave vehicular communication to support massive automotive sensing," *IEEE Communications Magazine*, vol. 54, no. 12, pp. 160–167, 2016.

[16] M. Yang, S.-W. Jeon, and D. K. Kim, "Interference management for in-band full-duplex vehicular access networks," *IEEE Transactions on Vehicular Technology*, vol. 67, no. 2, pp. 1820–1824, 2017.

[17] C. Wang and Y. J. Chun, "Stochastic geometry modeling and analysis for thz-mmwave hybrid iot networks," *arXiv preprint arXiv:2103.11674*, 2021.

[18] S. Farrag, E. Maher, A. El-Mahdy, and F. Dressler, "Outage probability analysis of uav assisted mobile communications in thz channel," in *2021 16th Annual Conference on Wireless On-demand Network Systems and Services Conference (WONS)*, IEEE, 2021, pp. 1–8.

[19] Q. Wei, L. Wang, Z. Feng, and Z. Ding, "Wireless resource management in lte-u driven heterogeneous v2x communication networks," *IEEE Transactions on Vehicular Technology*, vol. 67, no. 8, pp. 7508–7522, 2018.

[20] Y. Cai, Q. Zhang, and Z. Feng, "Qos-guaranteed radio resource scheduling in 5g v2x heterogeneous systems," in *2019 IEEE Globecom Workshops (GC Wkshps)*, IEEE, 2019, pp. 1–6.

[21] A. Saeed, O. Gurbuz, and M. A. Akkas, "Terahertz communications at various atmospheric altitudes," *Physical Communication*, vol. 41, p. 101 113, 2020.

[22] H. Zhang, H. Zhang, J. Dong, V. C. Leung, *et al.*, "Energy efficient user clustering and hybrid precoding for terahertz mimo-noma systems," in *ICC 2020-2020 IEEE International Conference on Communications (ICC)*, IEEE, 2020, pp. 1–5.

[23] S. A. Busari, K. M. S. Huq, S. Mumtaz, J. Rodriguez, Y. Fang, D. C. Sicker, S. Al-Rubaye, and A. Tsourdos, "Generalized hybrid beamforming for vehicular connectivity using thz massive mimo," *IEEE Transactions on Vehicular Technology*, vol. 68, no. 9, pp. 8372–8383, 2019.

[24] M. K. Samimi and T. S. Rappaport, "3-d millimeter-wave statistical channel model for 5g wireless system design," *IEEE Transactions on Microwave Theory and Techniques*, vol. 64, no. 7, pp. 2207–2225, 2016.

[25] A. F. Molisch, F. Tufvesson, J. Karedal, and C. F. Mecklenbrauker, "A survey on vehicle-to-vehicle propagation channels," *IEEE Wireless Communications*, vol. 16, no. 6, pp. 12–22, 2009.